Supplement of Atmos. Chem. Phys., 24, 10261–10278, 2024
https://doi.org/10.5194/acp-24-10261-2024-supplement


Atmospheric Chemistry and Physics
Open Access
EGU

*Supplement of*

# Cluster-dynamics-based parameterization for sulfuric acid–dimethylamine nucleation: comparison and selection through box and three-dimensional modeling

**Jiewen Shen et al.**

*Correspondence to:* Shuxiao Wang (shxwang@tsinghua.edu.cn)

**Assessing the reliability of the conventional treatment of gas-cluster-aerosol interactions in WRF-Chem/R2D-VBS simulations.**

Olenius and Roldin (2022) provided insights on the potential impact of gas–cluster–aerosol dynamics on NPF simulation using chemical transport models. Among various standard treatments of gas–cluster–aerosol dynamics in chemical transport modeling, they highlighted the assumption of instantaneous steady-state nucleation at every model time step as a potential source of bias. In response to this, we conducted a reliability assessment of steady-state nucleation in our WRF-Chem/R2D-VBS simulations. We evaluated the validity of the steady-state nucleation assumption by considering the system's e-folding time (time for clusters to reach (1-1/e) of their terminal concentration, following Li et al., (2023)). Specifically, we deemed the assumption reasonable if, under certain atmospheric conditions, the system's e-folding time is less than the simulation time step (300 s).

As shown in Figure S14, results indicates that the e-folding time does not show a significant correlation with $J_{1.4}$. Under the majority of atmospheric conditions (77.3%), the nucleating system's e-folding time is less than 300 s. Instances where the e-folding time exceeds 300 s are primarily observed in winter clean conditions characterized by low temperature (T < ~270 K), low condensation sink (CS < ~0.003 $s^{-1}$), and low precursor concentrations (SA < ~$10^6$ $cm^{-3}$). These findings align with the observations of Olenius and Roldin (2022). It's important to emphasize that this e-folding time represents the duration required for the system to transition from having only precursor molecules to reaching near-equilibrium concentrations of various clusters. In reality, cluster concentrations generally do not start from zero. Therefore, the calculated e-folding time serves as an upper limit estimate. Given the predominance of atmospheric conditions where the e-folding time falls within or below the simulation time step of 300 s, consequently, the steady-state treatment is generally deemed reasonable for our WRF-Chem/R2D-VBS simulations.

We further investigated another common treatment that may introduce bias: neglecting cluster formation in consuming precursor during nucleation. Our examination focused on assessing the proportion of precursor consumption by cluster formation relative to precursor concentrations. As shown in Figure S15 and S16, we found that this proportion increases with $J_{1.4}$ for both SA and DMA. Under the majority of atmospheric conditions (82.0% for DMA and 57% for SA), proportions are below 10%. Proportions exceed 10% are predominantly observed in scenarios also characterized by low temperature (T < ~270 K) and low condensation sink (CS < ~0.003 $s^{-1}$), but with high deference in concentrations between DMA and SA. Specifically, elevated SA concentrations, which lead to significant DMA consumption through cluster formation, and vice versa, contribute to scenarios where precursor consumption by cluster formation exceeds 10%. It's noteworthy that our calculation of precursor consumption by cluster formation starts from zero cluster concentration. Also, in the real atmosphere, cluster concentrations are generally nonzero, leading to another

upper limit estimate. Therefore, based on our analysis, it can be inferred that cluster formation may not introduce significant bias into NPF simulations under typical atmospheric conditions.

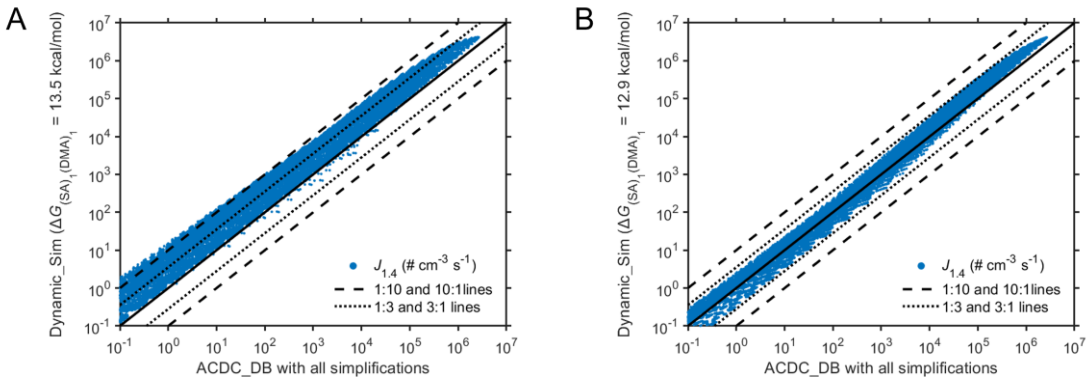


**Figure S1.** Comparison of $J_{1.4}$ predictions between ACDC_DB with all simplifications and Dynamic_Sim with different $\Delta G$ for initial $(SA)_1(DMA)_1$ cluster. A: $\Delta G$ = -13.5 kcal/mol; B: $\Delta G$ = -12.9 kcal/mol (Ning et al. 2024). Solid dots represent simulated $J_{1.4}$ values, solid lines indicate a 1:1 line, dotted lines correspond to 1:3 and 3:1 lines, and dashed lines represent 1:10 and 10:1 lines.

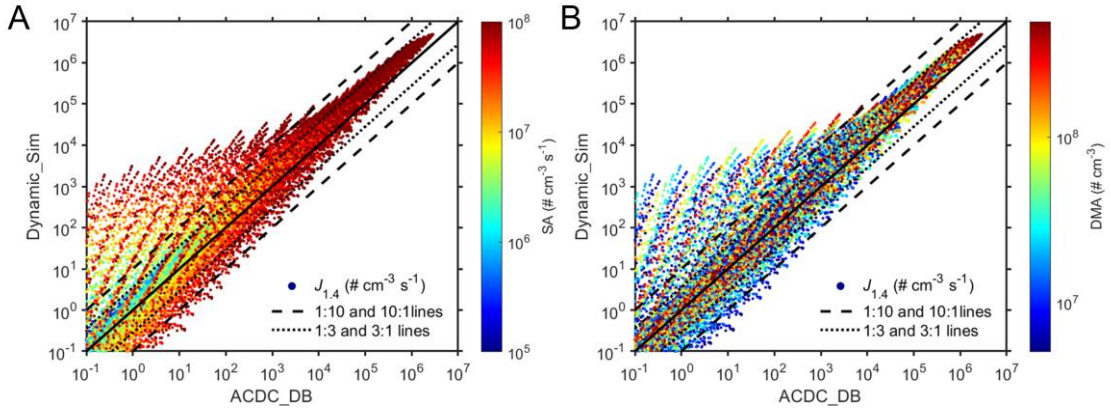


**Figure S2.** Comparison of $J_{1.4}$ predictions between ACDC_DB and Dynamic_Sim correlated with [SA] variation (A) and [DMA] variation (B). Solid dots represent simulated $J_{1.4}$ values, solid lines indicate a 1:1 line, dotted lines correspond to 1:3 and 3:1 lines, and dashed lines represent 1:10 and 10:1 lines.

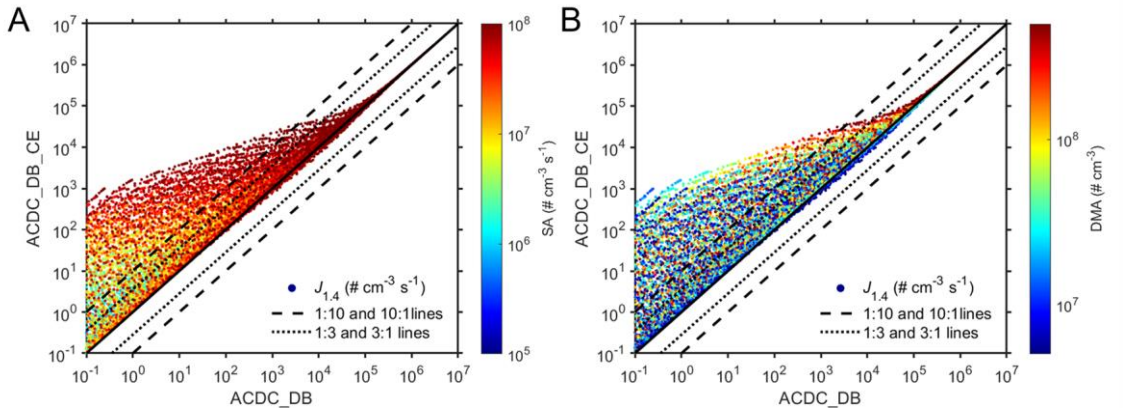


**Figure S3.** Same as Figure S2 but for ACDC_DB_CE.

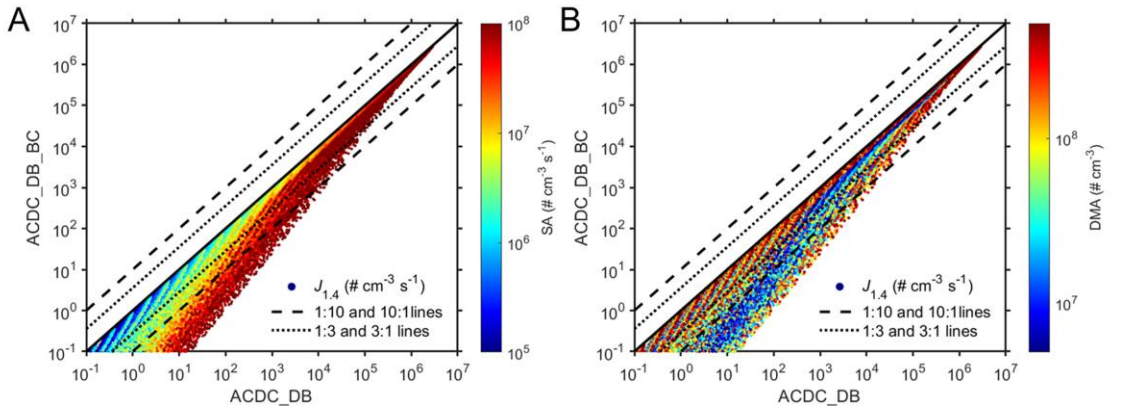


**Figure S4.** Same as Figure S2 but for ACDC_DB_BC.

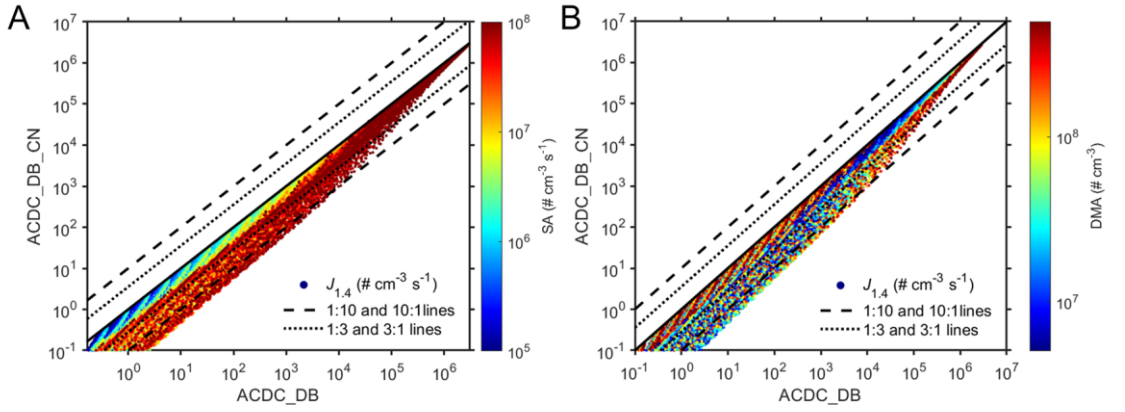


**Figure S5.** Same as Figure S2 but for ACDC_DB_CN.

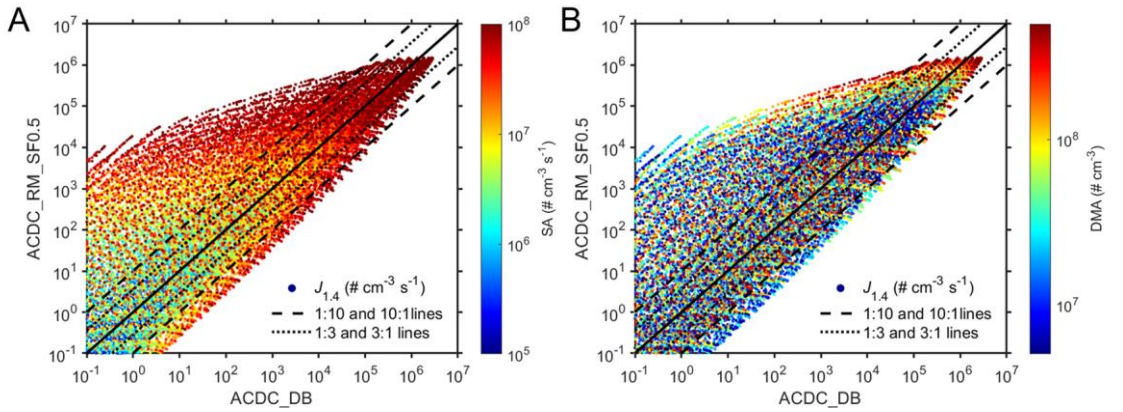


**Figure S6.** Same as Figure S2 but for ACDC_RM_SF0.5.

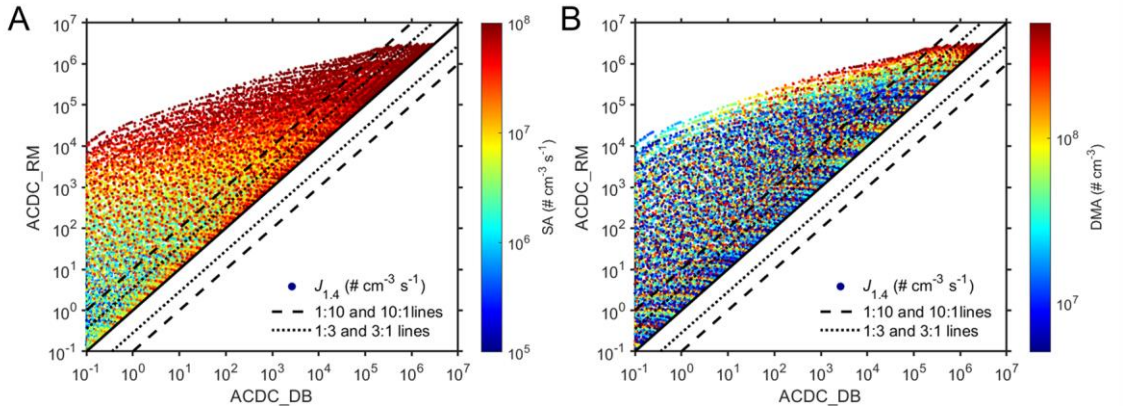


**Figure S7.** Same as Figure S2 but for ACDC_RM.

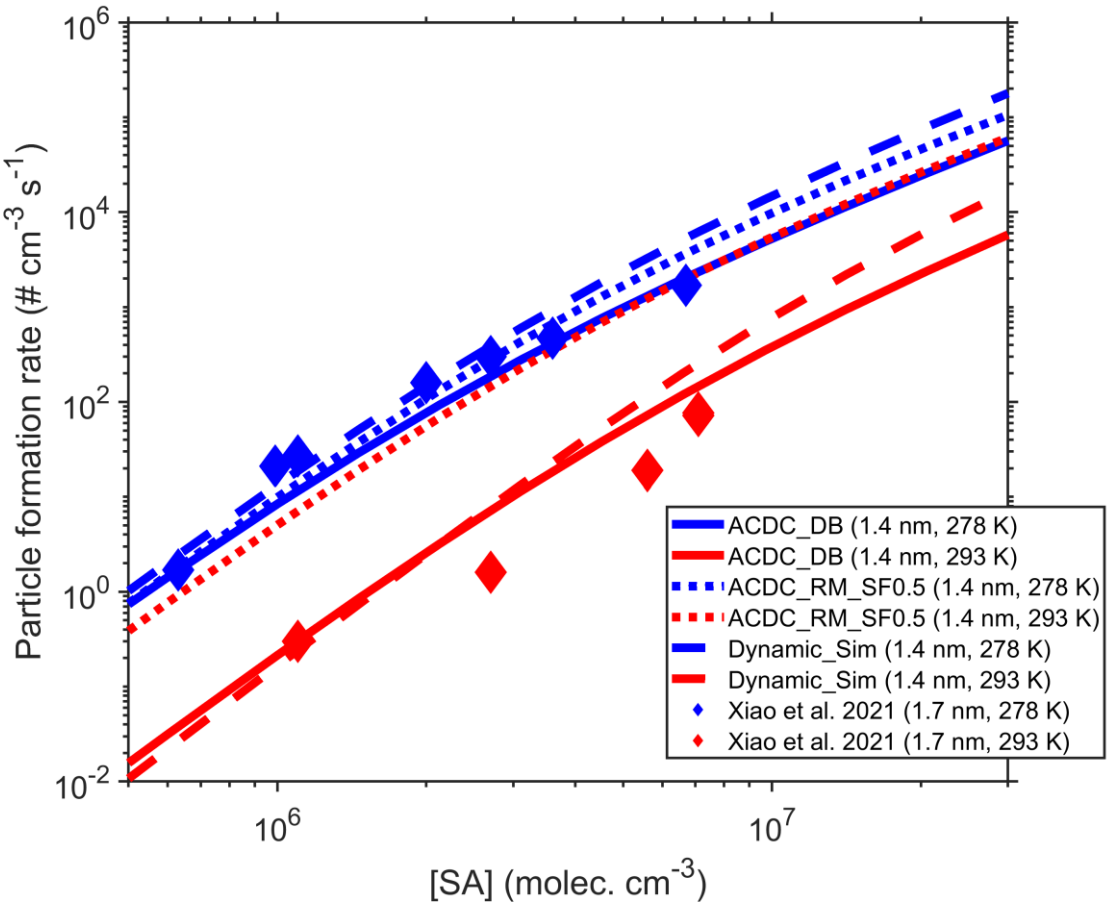


**Figure S8.** Comparison of modeled particle formation rates with measurements from CLOUD chamber experiments conducted by Xiao et al. 2021. Blue lines or diamonds represent particle formation rates at 278 K, while red ones represent those at 293 K; solid, dotted, and dashed lines denote the simulated results of ACDC_DB, ACDC_RM_SF0.5, and Dynamic_Sim, respectively. The simulations were conducted following the experimental conditions of Xiao et al. 2021, with specific conditions provided in their Table S1 and Table S2. It is noteworthy that Xiao et al. 2021 reported particle formation rates at 1.7 nm, whereas our simulations are at 1.4 nm. This discrepancy may lead to a slight overestimation of the simulated particle formation rates for simulations compared to the experiments. However, in the experiments, ~1 ppbv $NH_3$ was involved besides DMA during nucleation, which might enhance nucleation rates somewhat even through DMA is the dominant enhancing agent for SA-driven nucleation. Therefore, the two effects could partly offset each other, allowing for a direct comparison of particle formation rates between simulations and measurements.

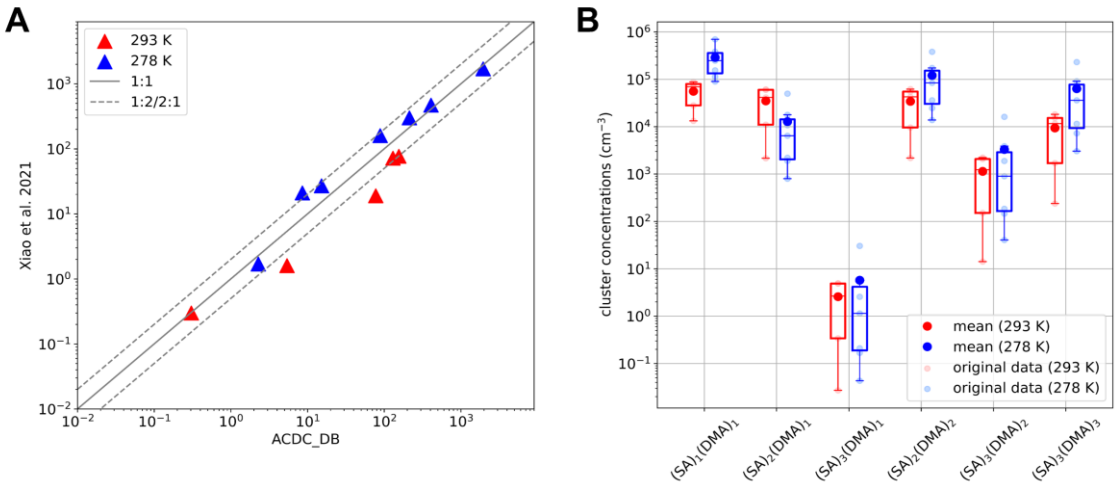


**Figure S9**. Comparison of measured $J_{1.7}$ from Xiao et al. 2021 and simulated $J_{1.4}$ using ACDC_DB with corresponding DMA concentrations in experiments (A), and the comparison of cluster concentrations at 293 K and 278 K (B).

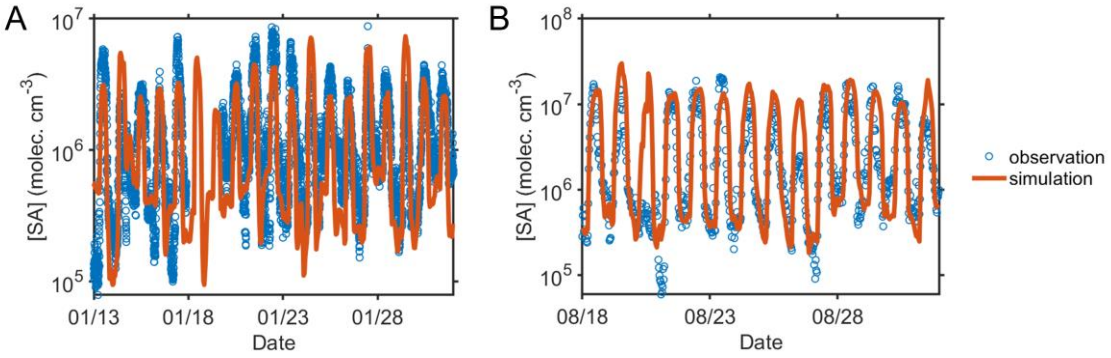


**Figure S10.** Comparison of simulated and observed SA concentrations. A for January and B for August 2019.

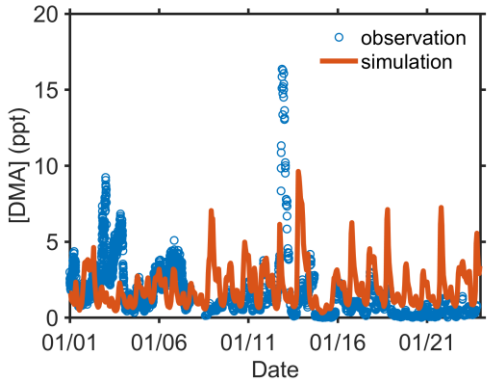


**Figure S11.** Comparison of simulated and observed DMA concentrations in January 2019. Only data for winter month (January 2019) is available.

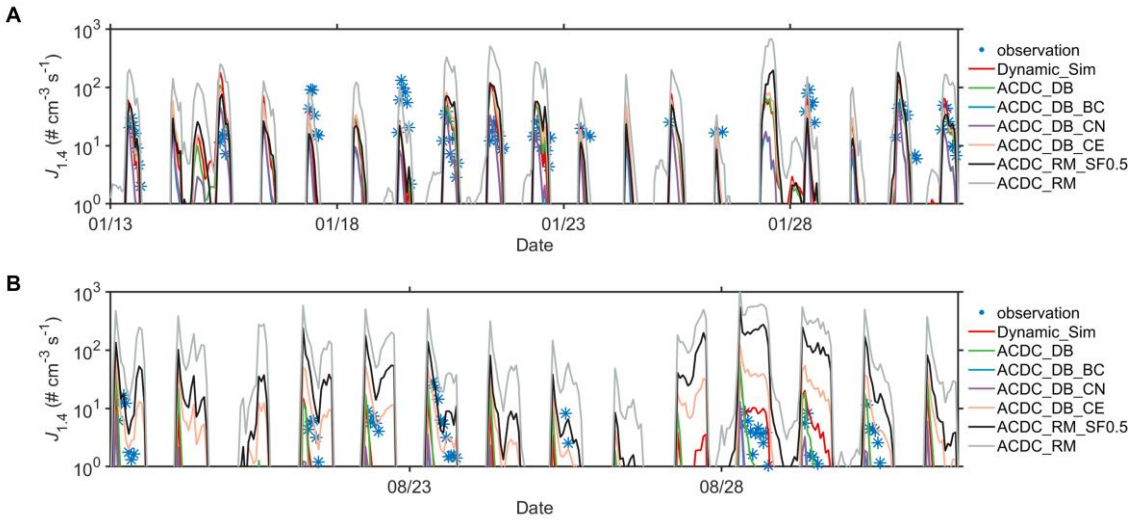


**Figure S12.** Comparison of simulated particle formation rates with those derived from field measurements during (A) January 13, 2019, to January 31, 2019, and (B) August 18, 2019, to August 31, 2019, in Beijing.

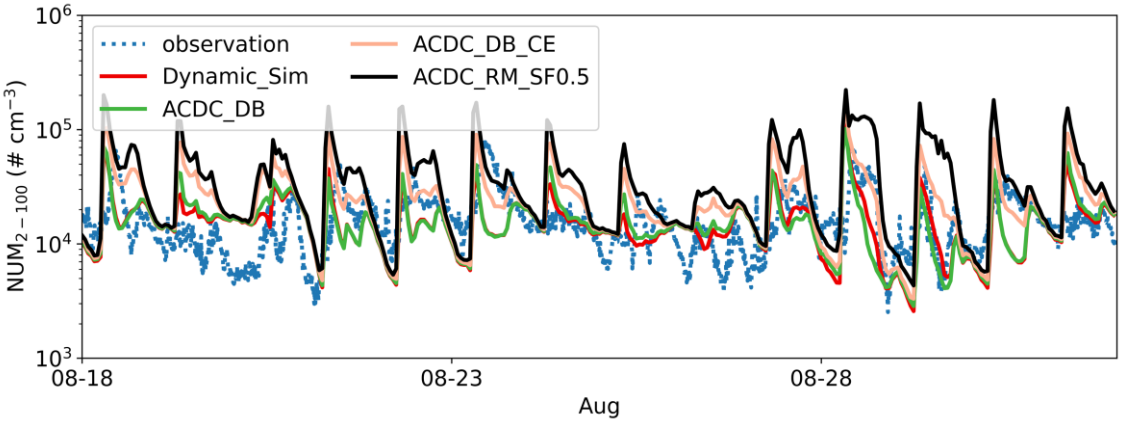


**Figure S13**. Comparison of observed and simulated aerosol number concentration within 2-100 nm during August 18, 2019, to August 31, 2019, in Beijing. Simulations are conducted using parameterizations of Dynamic_Sim, ACDC_DB, ACDC_DB_CE, and ACDC_RM_SF0.5.

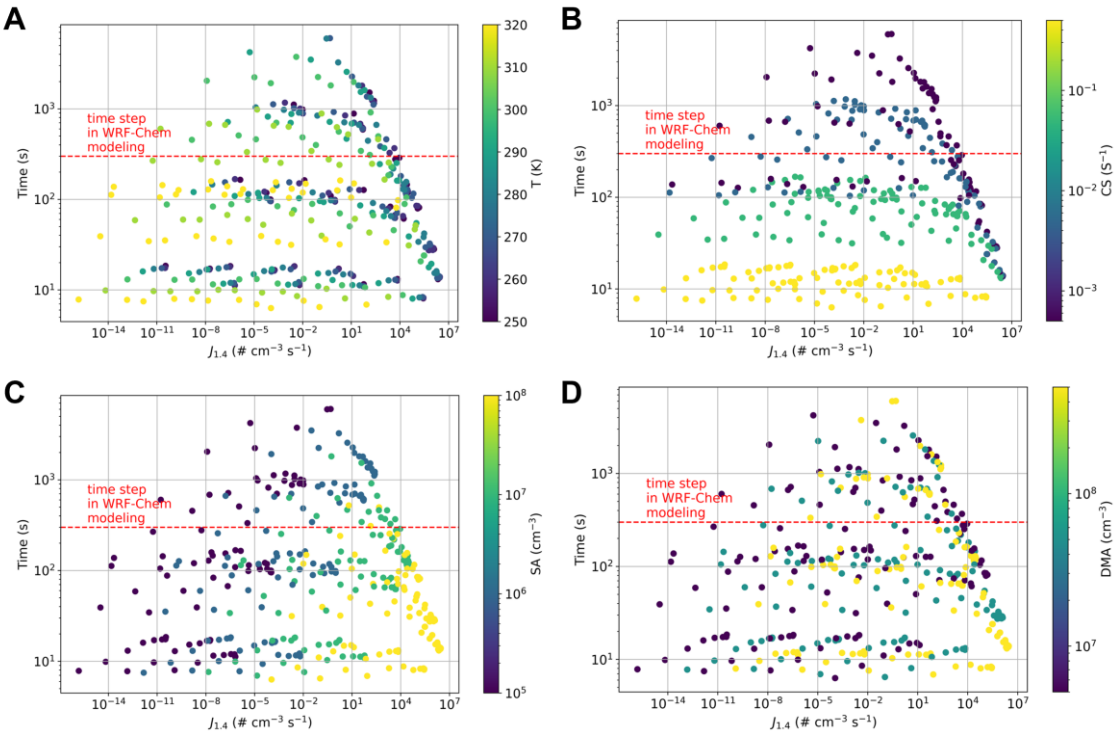


**Figure S14.** The variation of e-folding time with $J_{1.4}$ correlated with temperature (A), CS (B), SA concentration (C), and DMA concentration (D). The data points were calculated using a more sparse sequence of input parameters (T: 250, 260, 270, 280, 290, 300, 310, 320 (K); CS: $5.00 \times 10^{-4}$, $5.00 \times 10^{-3}$, $5.00 \times 10^{-2}$, $5.00 \times 10^{-1}$ ($s^{-1}$); SA: $1.00 \times 10^{5}$, $1.00 \times 10^{6}$, $1.00 \times 10^{7}$, $1.00 \times 10^{8}$ ($cm^{-3}$); DMA: $5.00 \times 10^{6}$, $5.00 \times 10^{7}$, $5.00 \times 10^{8}$ ($cm^{-3}$)) compared to those shown in Table S1.

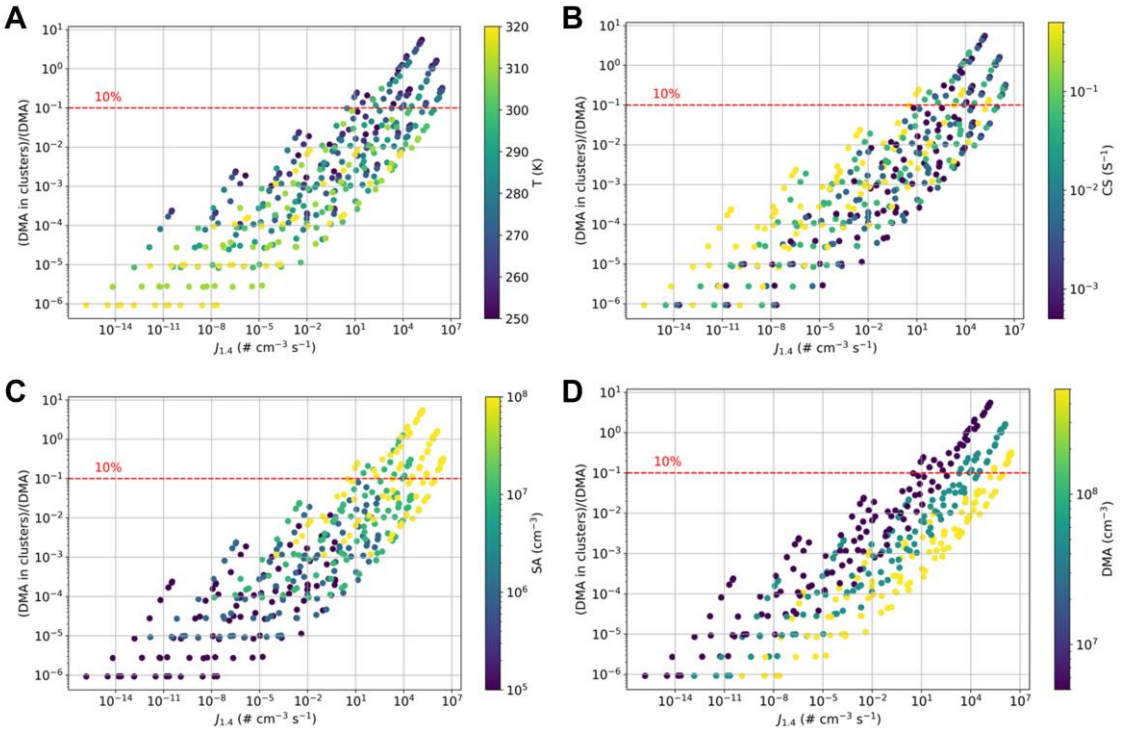


**Figure S15**. The variation of proportion of DMA consumption by cluster formation relative to precursor concentrations with $J_{1.4}$, correlated with temperature (A), CS (B), SA concentration (C), and DMA concentration (D). The input variables are consistent with Figure S14.

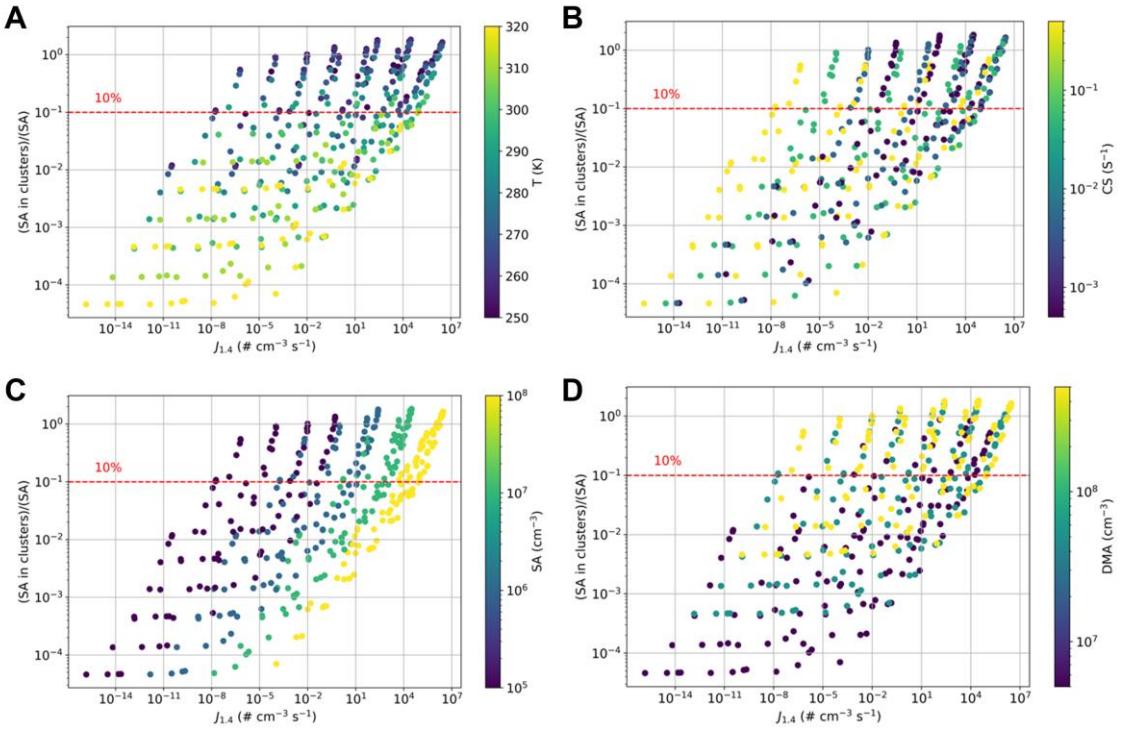

**Figure S16**. The variation of proportion of SA consumption by cluster formation relative to precursor concentrations with $J_{1.4}$, correlated with temperature (A), CS (B), SA concentration (C), and DMA concentration (D). The input variables are consistent with Figure S14.

**Table S1.** The ranges, total numbers and values at each point for the input parameters in deriving look-up tables

| | Range | Number of points | Values at each point |
|---|---|---|---|
| $T$ (K) | 250 – 320 | 15 | $250 + 5\times i$, $i = 0,14$ |
| CS ($s^{-1}$) | $5 \times 10^{-4} – 5 \times 10^{-1}$ | 16 | $5 \times 10^{-4} \times 10^{0.2\times i}$, $i = 0,15$ |
| [SA] (# $cm^{-3}$) | $1 \times 10^{5} – 1 \times 10^{8}$ | 16 | $1 \times 10^{5} \times 10^{0.2\times i}$, $i = 0,15$ |
| [DMA] (# $cm^{-3}$) | $5 \times 10^{6} – 5 \times 10^{8}$ | 11 | $5 \times 10^{6} \times 10^{0.2\times i}$, $i = 0,10$ |

**Table S2.** Comparison of simulated and observed concentrations of the nucleating precursors.

| **Precursor** | **Time period** | **Site** | **Simulation** | **Observation** | **Bias** | **NMB** |
|---|---|---|---|---|---|---|
| **SA (#/cm$^3$)** | 2019.01.13-2019.01.31 | Beijing | $1.35\times10^{6}$ | $1.47\times10^{6}$ | $1.20\times10^{5}$ | -10.80% |
| | 2019.08.18-2019.08.31 | | $5.74\times10^{6}$ | $3.51\times10^{6}$ | $2.23\times10^{6}$ | 14.32% |
| **DMA (pptv)** | 2019.01.01-2019.01.31 | Beijing | 1.96 | 1.98 | -0.02 | -10.96% |

## REFERENCES


Li, Y., Shen, J., Zhao, B., Cai, R., Wang, S., Gao, Y., Shrivastava, M., Gao, D., Zheng, J., Kulmala, M., and Jiang, J.: A dynamic parameterization of sulfuric acid–dimethylamine nucleation and its application in three-dimensional modeling, Atmospheric Chemistry and Physics, 23, 8789-8804, 10.5194/acp-23-8789-2023, 2023.

Olenius, T. and Roldin, P.: Role of gas-molecular cluster-aerosol dynamics in atmospheric new-particle formation, Sci Rep, 12, 10135, 10.1038/s41598-022-14525-y, 2022.

Xiao, M., Hoyle, C. R., Dada, L., Stolzenburg, D., Kürten, A., Wang, M., Lamkaddam, H., Garmash, O., Mentler, B., Molteni, U., Baccarini, A., Simon, M., He, X.-C., Lehtipalo, K., Ahonen, L. R., Baalbaki, R., Bauer, P. S., Beck, L., Bell, D., Bianchi, F., Brilke, S., Chen, D., Chiu, R., Dias, A., Duplissy, J., Finkenzeller, H., Gordon, H., Hofbauer, V., Kim, C., Koenig, T. K., Lampilahti, J., Lee, C. P., Li, Z., Mai, H., Makhmutov, V., Manninen, H. E., Marten, R., Mathot, S., Mauldin, R. L., Nie, W., Onnela, A., Partoll, E., Petäjä, T., Pfeifer, J., Pospisilova, V., Quéléver, L. L. J., Rissanen, M., Schobesberger, S., Schuchmann, S., Stozhkov, Y., Tauber, C., Tham, Y. J., Tomé, A., Vazquez-Pufleau, M., Wagner, A. C., Wagner, R., Wang, Y., Weitz, L., Wimmer, D., Wu, Y., Yan, C., Ye, P., Ye, Q., Zha, Q., Zhou, X., Amorim, A., Carslaw, K., Curtius, J., Hansel, A., Volkamer, R., Winkler, P. M., Flagan, R. C., Kulmala, M., Worsnop, D. R., Kirkby, J., Donahue, N. M., Baltensperger, U., El Haddad, I., and Dommen, J.: The driving factors of new particle formation and growth in the polluted boundary layer, Atmospheric Chemistry and Physics, 21, 14275-14291, 10.5194/acp-21-14275-2021, 2021.